Design and control of a novel robotic microsurgical forceps for Transoral Laser Microsurgery

Manish Chauhan, Nikhil Deshpande, Giacinto Barresi, Claudio Pacchierotti, Domenico Prattichizzo, Darwin Caldwell, Leonardo Mattos

Design and control of a novel robotic microsurgical forceps for Transoral Laser Microsurgery

Manish Chauhan[1], Nikhil Deshpande[1], Giacinto Barresi[1], Claudio Pacchierotti[2],
Domenico Prattichizzo[1], Darwin G. Caldwell[1], and Leonardo S. Mattos[1]
[1]Department of Advanced Robotics, Istituto Italiano di Tecnologia (IIT), Via Morego 30, Genova, 16163, Italy.
[2]CNRS at Irisa and Inria Rennes Bretagne Atlantique, Campus de Beaulieu, 35042 Rennes cedex, France.
Email: manish.chauhan@iit.it

***Abstract*— This paper presents a master-slave configuration robotic microsurgical forceps, which is capable of performing micro tissue manipulation. The master, i.e., 7 degree of freedom (DOF) device (*Sigma.7*), tele-operates the slave device which is a combination of a 6-DOF serial robotic arm and a 1-DOF (open/close) microsurgical forceps device. The serial robotic arm is used for positioning and orienting the slave device, which is integrated with a force/torque sensor for tissue grip-force measurement. This integrated system is analyzed for its (i) functional, (ii) usability, and (iii) haptic performance through user trials. The proposed system offers improved tool placement, enhanced tissue perception, safety, and accuracy with respect to the state of the art. This study the feasibility of replacing traditional manual forceps with easy-to-use and ergonomic robot-assisted devices.**

I. Introduction

Transoral Laser Microsurgery (TLM) deals with treatment of malignancies in the laryngeal region such as cysts, polyps, nodules, carcinoma by accessing the vocal cords (surgical site) through the larynx, which has the shape of an irregular closed cylinder. This shape offers a wide range of challenges to the surgeons which are broadly due to three factors, (i) **Surgical site**: difficulty in accessing its areas due to its limited size ranging between 17-21*mm* for males and 11-15*mm* for females [1], (ii) **Surgical tools**: one DOF long (length $200-240mm$ exclusive of tool handle, diameter $2-2.5mm$) rigid structure tools, and (iii) **Surgeon interface**: manual handling makes it unwieldy for surgeons to perform intraoperative task ergonomically.

Figure 1 shows the exposure method of the surgical site using a laryngoscope (approximate length of 180*mm* and cross-section $16 \times 23mm^2$) which is inserted orally for obtaining direct line-of-sight through the surgical microscope. A CO_2 laser beam is aimed from a distance of 400*mm* with the help of a mechanical micro-manipulator joystick. The combination of the laryngoscope and micro-manipulator consumes a depth of $300-340mm$. This leaves the surgeons with a narrow range of $50-60mm$ range for microsurgical tool movement and tissue manipulation. Additionally, manual handling of these tools induces hand tremors which makes it cumbersome and non-ergonomic for accessing and resecting the vocal folds [2].

With a focus on improving the surgeon-machine interface, the research in this paper extends the benefits of robot-assisted technologies to the critical aspect of tissue manipulation in TLM and presents the design and development of a novel, robotic microsurgical forceps with the surgeon using an ergonomic interface with haptic feedback for improved surgical perception and task outcome. Earlier research in this context resulted in the design of a robot-assisted forceps device presented in [3]. However, in using the device in a realistic surgical scenario, key issues were identified related to the size of the device, which caused occlusion of the surgical site. The device presented in this paper focuses on resolving these issues and meeting the dimensional and operational constraints of TLM through the design of a next generation robotic forceps for enhancing the performance, accuracy & safety of the surgery.

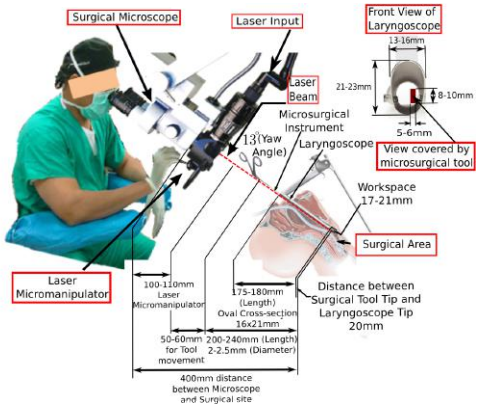

Fig. 1: Traditional constraints in TLM operating room.

II. Related Work

Various robot-assisted surgical tools have been developed by different groups. Snake-like manipulators with high tip dexterity for tissue manipulation and suturing [4] have been explored by Simaan et al. A cooperatively controlled bimanual teleoperation robot having 3-DOF wrists with surgical tools attached was developed by He et al.[5]. Wang et al. [6] presented a new robot-assisted master-slave laryngeal surgery system consisting of two symmetrical 9-DOF manipulators, with quick-change interface for surgical tools. Rivera-Serrano et al. [7] presented a highly articulated robot in a follow-the-leader mechanism using a master controller.

Solares and Strome [8] and Desai et al. [9] have explored the utility of the *da Vinci Surgical System* [10] for TLM but found size of the *da Vinci* tool shafts as a major limitation along with constant change of attendant during surgery. An effective solution was presented by Maier et al. [11] where standard surgical tools could be attached to a lightweight manipulator without any modification. Despite extensive research efforts, these instruments are not particularly focused towards TLM application. Also, surgeon performance can be enhanced with haptic feedback for enhanced intra-operative perception [12],[13]. These benefits lend themselves readily towards facilitating and improving the complex suite of oto-laryngological techniques of tool control involved in TLM. Having understood these needs, it is important to create a device with such capability.

III. Robot-assisted Microsurgical Forceps Design

With reference to above discussion, a standalone device for improved motion accuracy, reduced operator dependence, and simpler tissue manipulation with surgical exposure was created while complying with design constraints as noted in Fig. 1. The key design specifications of these components are based on the constraints offered by TLM which are listed in Table I. The novel design consists of three modules: (i) the tool shaft; (ii) the tool actuation mechanism; and (iii) the tool-shaft holder.

TABLE I: Design specifications of the microsurgical forceps

Design Limits	Remarks
Tool maneuverability range of 70-80*mm*.	To be operable under the surgical microscope.
Displacement from microscope line-of-sight of 200*mm*.	For avoiding interference between tool and other surgical setup.
Tool footprint under microscope of 5*mm*.	To maintain minimum vision occlusion through the microscope.

A. The tool shaft

This component is a modified version of the traditional microsurgical tools, made up of an outer shaft (ϕ 2*mm*) which holds an inner translating wire (*itw*,ϕ 1*mm*). The translation of this wire ($\approx$ 3*mm*) provides the open-close DOF of the tool jaw. The tool shafts are of two types: (i) where pushing action of the *itw* closes the tool jaws, and (ii) where pulling action of the *itw* closes the jaws. One adaptation, namely docking interface (*DI*) is introduced at the proximal end of the tool shaft which is a short hollow tube with *M*3 external threading. (Refer Fig. 2(a)).

B. Tool actuation mechanism

The tool actuation mechanism consists of a set of five linkages ("L1","L2", "L3", "L4", "L5"), which are designed to provide linear translation of the *itw* through kinematic inversion. Here, the link "L1" is treated as ground, i.e., the hinge link. Link "L2" forms the input link (i.e., slider) along the *"actuator axis*" for transfering motion to link "L3" which in-turn transfers motion to link "L4" through the ground/hinge link "L1". Links "L3" and "L4" have an inverse relationship and Link "L4" is directly coupled with link "L5". Link "L5" (i.e., wire pusher) is connected to and actuates the *itw* of the tool shaft along the "*tool axis*" (Refer Fig. 2(b)). A force sensor (ATI Nano17) is located with its measurement axis coincident with the *"actuator axis*" of link "L2" optimally for allowing the sensing of the tissue gripping force. The closing of the gripper jaws (along *"tool axis*") on tissue transmits a reaction force on to the surface of the sensor through the link "L2" (along *"actuator axis*"). The force sensor, attached to link "L2", outputs a signal in direct proportion to the tissue gripping force.

C. Tool-shaft holder

Figure 2(c) shows the design of the tool-shaft holder which connects the tool shaft with tool actuation mechanism. It's frame comprises of three sub-frames "F1", "F2", and "F3". The tool shaft itself is attached rigidly to sub-frame "F1" through *DI* at point "P1" such that the "*tool axis*" is at an offset of 200*mm* from the *"actuator axis*". The cross-sectional thickness of "F1" is designed to be 5*mm*. Both these aspects are maintained to comply with the design constraints in Table I. Further, the sub-frames "F1" and "F2" are rigidly connected at "P2" (i.e. *"support axis*"). The sub frame "F3" is designed as an attachment bracket for robot end effector upon which a linear actuator (Nanotec L2018 series) is placed to drive the open/close DOF.

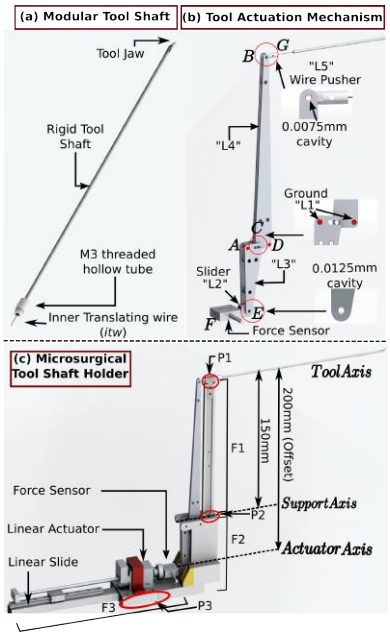

Fig. 2: Robot assisted Microsurgical forceps design.

IV. The novel straight-line mechanism and its validation with ADAMS simulation

The tool open/close DOF is actuated by a mechanism which is designed as a graphical synthesis method in two-stages. This five-link mechanism is synthesized as a Function

Generator [14] problem (where output motion is linearly related to input actuation) to provide straight line motion of the *itw*.

1) In the first stage of synthesis, a suitable three link mechanism is formed which can allow linear displacement of the slider (i.e., link "L2": F-E) within limits (x_i, x_f) along the *"actuator axis"*. Here x_i and x_f are the initial and final positions of slider motion, i.e., 0 and $3mm$ respectively. The kinematic synthesis begins with an arbitrary choice of hinge point A at an offset of $50mm$ from the *"actuator axis"* in Y-direction. (Refer Fig. 3). On the *"support axis"* another point C is chosen at a distance of $10mm$ from point A in X-direction. The end point E of link "L2" is chosen on the *"actuator axis"* such that its position lies on the vertical line passing through point A. Joining the three points $A-C-E$, a triangular shaped link is achieved, named as "L3". The linear displacement of link "L2" causes link "L3" to translate in angular motion (θ_i, θ_f). For ensuring straight-line trajectory of link "L2" between x_i and x_f, three additional intermediate Chebyshev's precision points [12] are chosen using the equation 1.

$$x_j = a - h\cos[(2j-1)\cdot\pi/2n] \qquad j = 1, 2, 3 \qquad (1)$$

The variables a and h are defined as $(x_i + x_f)/2$ and $(x_f - x_i)/2$ respectively. The choice of three Chebyshev's precision points (n) is sufficient for allowing the slider to follow an exact straight line path. The three precision points are $x_1 = 0.2mm$, $x_2 = 1.5mm$ and $x_3 = 2.799mm$. The link "L2" starts from x_i passes through the three precision point x_1, x_2, x_3 & finishes its stroke at its final position x_f. Since link "L2" is rigid, points F and E have identical movement such that displacement of link "L2" causes angular motion of link "L3" through corresponding positions $(\theta_i, \theta_1, \theta_2, \theta_3, \theta_f)$. A closer observation of link "L3" $(A-C-E)$ shows that a displacement of $1mm$ of end point E in X direction (Fig. 4(a)) causes its simultaneous displacement of $0.0130mm$ in Y direction (Refer Fig. 4(b)). This negligible Y displacement is because of angular motion of link "L3" with reference to the hinge point A which is compensated with a small cavity in link "L3" at end point E.

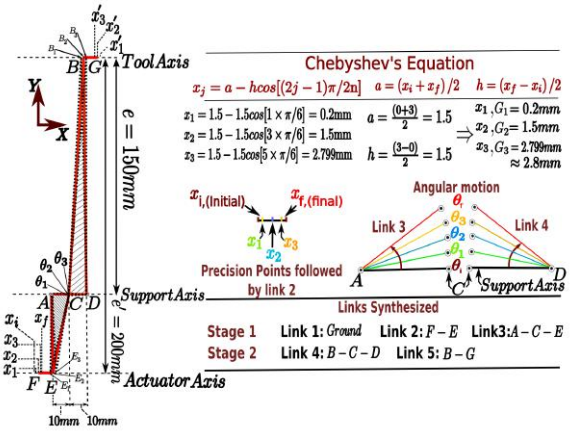

Fig. 3: Kinematic Synthesis of Mechanism for surgical tool actuation.

1) In the second stage of synthesis, two links are fabricated such that the motion from *"actuator axis"* can be transferred to *"tool axis"*. First, a hinge point D is chosen along *"support axis"* at a distance of $10mm$ from point C in X- direction. Another point B is assumed on the *"tool axis"* which is at a distance of $150mm$ from *"support axis"* in Y-direction. The triangular link $B-C-D$ so created is termed as link "L4". Point C serves as the common engagement point for links "L3" and "L4" such that the angular motion of link "L3" through $(\theta_i, \theta_1, \theta_2, \theta_3, \theta_f)$ is mirrored by link "L4" . The fifth link is synthesized to be connected at the end point B, link $B-G$ or "L5". The angular motion of link "L4" is transferred to "L5" such that it produces the corresponding straight line translation of the *itw* through the precision x_1', x_2', x_3'. The ratio of the link lengths "L4" and "L3" results in a *link-ratio* of 3. With this arrangement, a displacement of $1mm$ at end point E results in a displacement of $3mm$ at end point B which produces open/close of the forceps jaws. As was evident for point E of link "L3", here too,

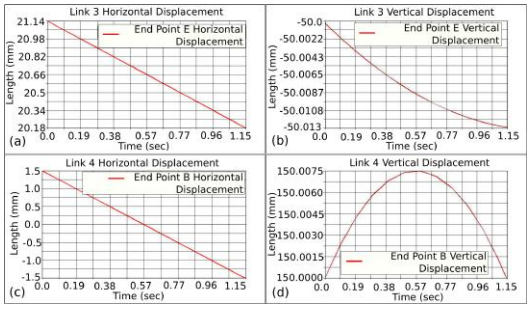

Fig. 4: Curvi-linear motion of Link 3 and 4.

the angular motion of point B causes a simultaneous X and Y displacement. Figure 4(d) shows this negligible displacement of $0.0075mm$ in Y direction which is compensated with a cavity in link "L4" at point B (Refer Fig. 2(b)).

On performing the mobility analysis using the Grbler's criterion [15], it was found that the mechanism's DOFs were *two*. Here, the first DOF is the linear translation of link "L5" $(B-G)$ and the second DOF can be explained as the negligible motion in the Y direction for the end points E and B. Finally, the angular movements of links "L3" and "L4" are possible in both clockwise and anticlockwise direction which makes it adaptable for both the types of microsurgical forceps as discussed in sec. III-A.

V. Integration and control of robot assisted device with serial manipulator

In continuation with the discussion in sec. III-C, the above designed device was integrated with a 6 DOF Univeral Robot serial manipulator (UR5 [16]) in order to position the tool exactly at the surgical site. Figure 5(a) and (b) shows the integration of this device with control through 7 DOF teleoperation master device (Force Dimension *Sigma.7* [17]).

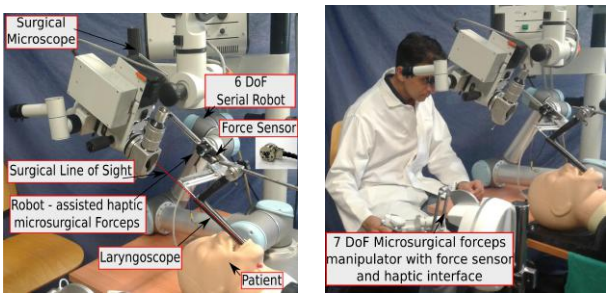

(a) Closeup view under surgical microscope. (b) Haptic feedback integration.

Fig. 5: Microsurgical forceps integration control by master slave configuration.

A. Control and haptic feedback Design

Linux-based software was written using the Robot Operating System platform for controlling the 7-DOF manipulator. The velocities of the robotic manipulator joints $\dot{q} \in \mathbb{R}^6$ can be expressed with unilateral velocity based control as:

$$\dot{\mathbf{q}}_\mathbf{r} = \mathbf{J}^{-1}\dot{\mathbf{q}}_\mathbf{h}\zeta \tag{2}$$

where $\mathbf{J}^{-1}$ is the Moore-Penrose pseudo-inverse of the manipulator Jacobian matrix $\mathbf{J} \in \mathbb{R}^{7x6}$ and $\dot{\mathbf{q}}_\mathbf{h} \in \mathbb{R}^7$ are the velocities of the *Sigma.7*'s end-effector. The gesture scaling factor ζ is tunable to allow coarse and fine gestures in different stages of operation. The $\dot{\mathbf{q}}_\mathbf{h}$ velocities of the master end-effector are scaled through a low-pass filter in equation (3), with a tunable factor β to control the level of high-frequency tremor suppression.

$$\dot{\mathbf{q}}_\mathbf{h}^k = (1-\beta)\cdot\dot{\mathbf{q}}_\mathbf{h}^{k-1} + \beta\cdot\dot{\mathbf{q}}_\mathbf{h}^{encoder} \tag{3}$$

Sigma.7's gripper DOF was mapped directly to the open/close DOF of the microsurgical forceps such that while a tissue is gripped with the forceps, the sensed value from the ATI sensor is filtered using a low-pass filter and then scaled for rendering to the 7^{th} (gripper) DOF of the *Sigma.7*. The following equations are used.

$$\begin{aligned} f_g^k &= (1-\beta)\cdot f_g^{k-1} + \beta\cdot f_g^{sensor} \\ f_g^{sigma} &= \kappa\cdot f_g^k \end{aligned} \tag{4}$$

The values used for the constants are emperically obtained as $\beta = 0.001$ and $\kappa = 4$. The haptic rendering loop is run at 500 Hz.

VI. Evaluation & user trials

User trials were conducted for establishing (i) the performance; (ii) the usability; and (iii) the gripping force feedback of the integrated device. 12 different subjects (divided in two sets A and B of 6 each) operated the master device for performing an experiment with ring-to-peg transfer (Refer inset, Fig. 6). This task was chosen due to its similarity in nature to the general surgical tasks like gripping, pulling and orienting a tissue out of the larynx. These trials were conducted under two conditions: (i) C1: with haptic feedback; and (ii) C2: without haptic feedback for obtaining a comparative analysis between the two conditions. "Set A" subjects performed trials in the sequence C2-before-C1, while "Set B" performed C1-before-C2 for avoiding subjective bias in the results coming from the order of presentation of the haptic condition. Each subject in both the set's performed 6 trials for accounting the learning aspects.

For uniform results, the UR5 robot was programmed to start from the home position in each trial where the following measurements were made, (i) Time required to lift the O-ring from a peg$\left(T_{lift}\right)$, (ii) Total time for peg to peg tansfer $\left(T_{total}\right)$, (iii) Number of attempts for lifting the ring, (iv) Number of ring drops during transfer, (v) the Trajectory executed for the task, and (vi) Tissue gripping force on the O-ring surface for C1 and C2 conditions (only for Set B).

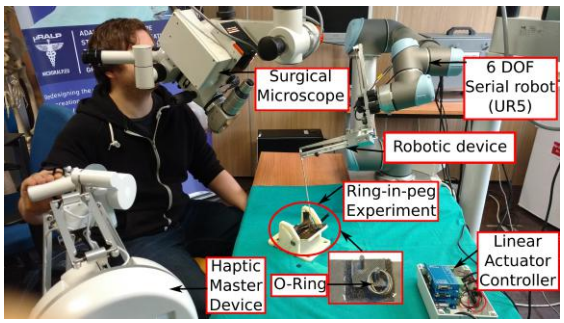

Fig. 6: Ring-in-peg experiment.

TABLE II: Evaluation statements

S1. The control of the device was precise.
S2. The control of the device induced fatigue in my hand.
S3. I had to work hard to accomplish the task with this device.
S4. The control/use of the device was easy.
S5. I found the device was easy to learn, so I could start using it quickly.
S6. I was stressed, irritated, and annoyed using this device during the task.
S7. I would like to use this device again for this kind of task.
S8. My performance in this task with this device was satisfying
S9. It was easy to make errors with this device.
CP. Preference of condition 1 or condition 2

(Age of subjects. Mean=27.75 years with SD=2.95 years. Gender. 9 Male, 3 Female)

A subject-wise experience evaluation was collected through a questionnaire of 9 statements (Refer Table II)

where their degree of agreement with each statement was collected along a 7-point Likert-type scale [16] (the score "1" means "I strongly disagree", while "7" implies "I strongly agree"). At the end, the subjects compared their overall experience by expressing a degree of condition preference (CP) for C1 or C2. Based on all the above measurements and subjective evaluations, the following section explains the results of the experiment.

A. Device Performance Analysis

1) Trajectory Analysis : Change in trajectory lengths (improvement or deterioration) over the trials performed by the subjects was chosen as a metric for making a comparison among subjects in order to establish the device performance. Since each subject performed 6 trials, the length ratio of the subsequent 5 trials was calculated against the first trial. It was found that the ratio of the last $\left(6^{th}\right)$ trial was **0.8273**, while the average ratio over the 5 trials was **0.9218**. Both values being less than 1 demonstrate quick learnability and skill acquisition of subjects over a small set of trials.

2) Execution Time Analysis: Analysis of task execution time showed that T_{lift} reduced from 72.17 seconds to 42.25 seconds over the 6 trials with an improvement of 41%. The same trend for T_{total} was obtained where it went from 94.4 seconds to 56.8 seconds, giving an improvement of almost 40%. This demonstrated that the device allowed quick learning and skill acquisition for subjects.

B. System Usability Analysis

1) User Accuracy evaluation: The subjective evaluation scores in Table III (S1, S7, S8, and S9) are observed to be greater than 4 on 7-point scale, indicating a positive evaluation of the device accuracy. For S1, the subjects evaluated the device at (**5.455 / 7**), giving high marks for its precision in the tasks. This aspect is also confirmed by S8 where the subjects are comfortable and satisfied with their performance using the device (**5.33 / 7**).

TABLE III: Scores for Questionnaire

	Subject Trials				
	C1		C2		Overall Scores
	m	sd	m	sd	m
S1	5.58	0.64	5.33	1.59	5.455
S2	3.00	1.73	2.41	0.86	2.705
S3	3.91	1.49	3.16	1.46	3.535
S4	4.91	1.11	4.58	1.65	4.745
S5	5.75	1.16	5.5	1.44	5.625
S6	2.25	1.23	2.66	1.02	2.451
S7	5.25	1.42	5.16	1.28	5.205
S8	4.91	1.55	5.75	1.16	5.33
S9	4.08	1.38	3.91	1.60	3.995
CP	m=4.08; sd = 2.09				

2) Usability Analysis: The overall scores for statements S2, S3, S4, S5, and S6 pertain to the overall usability, ergonomics, and usage fatigue. Low values on S2 and S6 indicate the reduced mental effort required by subjects, while the high scores on S4 and S5 indicate device easy to use and learnability.

C. Haptic Performance Analysis

1) Comparison of robot trajectory under C1 and C2: The comparative analysis show that the overall trajectory ratio in C1 was much lower than that for C2 condition. Also, irrespective of the order of presentation of the device, the average ratio of robot trajectory was smaller in C1 (**Set A** (C1:0.77, C2:0.9654) and **Set B** (C1: 0.8926, C2: 1.0592)). Though this value is not significantly smaller, it indicates a trend where haptic feedback prompts better performance with the robot.

2) Time comparison for task under C1 and C2:

1) T_{lift}: There was no significant difference between time response for each subject to lift a ring from a peg in both conditions with mean time of 55.7s for C1 and 57.8s for C2. A comparison of the number of attempts done to lift the ring (errors) show that the condition C1 is favorable (with 6 occurrences) with respect to C2 (with 9 occurrences).
2) T_{total}: No significant difference was seen in comparison of time response for pick-n-place of ring for both conditions with mean time of 71.8s for C1 and 73.5s for C2. Also, insignificant difference in number of ring drops (errors) after lifting were observed with 2 occurrences in C1 and 1 occurrence in C2.

3) Comparison of Gripping force in C1 and C2: Figure 7 show a subjective comparison of O-ring gripping force under conditions C1 and C2 for subjects in **Set B**. It can seen that the gripping force applied under condition C1 is significantly less in comparison to C2 indicating an awareness of the force required to grasp the ring in condition C1.

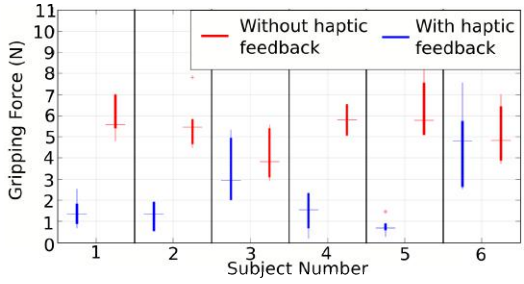

Fig. 7: Subject-wise comparison of gripping force.

In order to get a better perception while gripping with forceps, a comparison of average gripping force applied by subjects showed that the mean force applied on the ring was less in C1 (p = 7.4189e-04) according to *Student's t-test* with respect to C2 (2.158N vs 5.606N). This result indicates that gripping force feedback can allow enhanced perception as well as safety, limiting the force applied for tissue gripping.

This result agrees with the conclusion in [17]where the mean applied force was less under haptic feedback condition.

4) Subjective evaluation with questionnaire: The questionnaire scores in Table III were evaluated through Friedman test [18] to understand the effect of gripping force feedback on task completion time. It can be seen from statements S1, S2, S4, S5, S6 and S7 that the subjects were unable to judge the performance of device with respect to the two conditions. The performance parameters of the device i.e. its learning and induction of fatigue got higher scores in condition C1. But this score had no significant difference with respect to C2. Also, a comparison of scores for statement S3, S8 and S9 shows that device performance suffered marginally in context of errors occurring in condition C1.

VII. Conclusion and Future Work

This paper presents a novel design of an integrated robot-assisted microsurgical forceps tool for intraoperative use in TLM. The new design complies with the TLM constraints and replaces the traditional manually operated tools with a teleoperation system consisting of an integrated: (i) 7 DOF robotic microsurgical forceps; (ii) a 7-DOF teleoperation master device; and (iii) a force/torque sensor for tissue gripping feedback. A comparative performance analysis of the device was done through user trials under C1 and C2 conditions which resulted in better performance with force feedback. The system provides: (i) improved controllability, safety; (ii) reduced task completion time; (iii) enhanced surgical site perception; and (iv) intuitive and ergonomic use with a common surgeon interface providing gesture scaling, reduced hand tremors and wrist excursions. In future, an attempt to increase the tool workspace shall be investigated by addition of rotational DOF to tool shaft which shall be tested in collaboration with expert surgeons through ex-vivo and cadaver trials.

References

[1] M. Hirano, Morphological Structure of the Vocal Cord as a Vibrator and its Variations, Folia Phoniatrica et Logopaedica, vol. 26, pp. 89-94, 1974.

[2] P. A. Liverneaux, S. H. Berner, M. S. Bednar, S. J. Parekattil, G. M. Ruggiero, and J. C. Selber, Telemicrosurgery: robot-assisted microsurgery. Springer Science and Business Media, 2012.

[3] N. Deshpande, M. Chauhan, C. Pacchierotti, D. Prattichizzo, D. G.Caldwell, and L. S. Mattos, Robot-assisted microsurgical forceps with haptic feedback for transoral laser microsurgery, in Engineering in Medicine and Biology Society (EMBC), 2016 IEEE 38th Annual International Conference of the. IEEE, 2016, pp. 5156-5159.

[4] N. Simaan, R. Taylor, and P. Flint, A Dexterous System for Laryngeal Surgery, in Proc. Intl. Conf. on Robotics and Automation, (ICRA 2004), 2004, pp. 351-357.

[5] C. He, K. Olds, I. Iordachita, and R. Taylor, A New ENT Microsurgery Robot: Error Analysis and Implementation, in Proc. Intl. Conf. on Robotics and Automation, (ICRA 2013), 2013, pp. 1221-1227.

[6] S. Wang, Q. Li, J. Ding, and Z. Zhang, Kinematic Design for Robot-assisted Laryngeal Surgery Systems, in Proc. IEEE/RSJ Intl. Conf. on Intelligent Robots and Systems (IROS 2006), 2006, pp. 2864-2869.

[7] C. M. Rivera-Serrano, P. Johnson, B. Zubiate, R. Kuenzler, H. Choset, M. A. Zenati, S. Tully, and U. Duvvuri, A Transoral highly flexible robot: Novel technology and application, The Laryngoscope, vol. 122, no. 5, pp. 1067-71, 2012.

[8] C. A. Solares and M. Strome, Transoral Robot-assisted CO 2 Laser Supraglottic Laryngectomy: Experimental and Clinical Data, The Laryngoscope, vol. 117, no. 5, pp. 817-820, May 2007.

[9] S. C. Desai, C. K. Sung, D. W. Jang, and E. M. Genden, Transoral Robotic Surgery using a Carbon-dioxide Flexible Laser for Tumors of the Upper Aerodigestive Tract, The Laryngoscope, vol. 118, no. 12, pp. 2187-2189, Dec. 2008.

[10] da Vinci Surgical System. Intuitive Surgical Inc. CA, USA. Accessed on 07-Dec-2016, www.intuitivesurgical.com. [Online]. Available:www.intuitivesurgical.com

[11] T. Maier, G. Strauss, M. Hofer, T. Kraus, A. Runge, R. Stenzel, J. Gumprecht, T. Berger, A. Dietz, and T. C. Lueth, A New Micromanipulator System for Middle-Ear Surgery, in Proc. Intl. Conf. on Robotics and Automation, (ICRA 2010), 2010, pp. 1568-1573.

[12] L. Meli, C. Pacchierotti, and D. Prattichizzo, ?Experimental evaluation of magnified haptic feedback for robot-assisted needle insertion and palpation,? International Journal of Medical Robotics and Computer Assisted Surgery, 2017.

[13] Meli, Leonardo, Claudio Pacchierotti, and Domenico Prattichizzo. "Sensory subtraction in robot-assisted surgery: fingertip skin deformation feedback to ensure safety and improve transparency in bimanual haptic interaction." IEEE Transactions on Biomedical Engineering 61.4 (2014): 1318-1327.

[14] E. C. Kinzel, J. P. Schmiedeler, and G. R. Pennock, Function generation with finitely separated precision points using geometric constraint programming, Journal of Mechanical Design, vol. 129, no. 11, pp. 1185-1190, 2007.

[15] G. Gogu, Chebychev grubler kutzbachs criterion for mobility calculation of multi-loop mechanisms revisited via theory of linear transformations, European Journal of Mechanics-A/Solids, vol. 24, no. 3, pp. 427?441, 2005.

[16] Universal Robot 5. Universal Robots. Denmark. Accessed on 07-Dec-2016, http://www.universal-robots.com/products/ur5-robot/. [Online]. Available: http://www.universal-robots.com/products/ur5-robot/

[17] Force Dimension: Sigma 7, Product Overview. Accessed on 6th September 2016. [Online]. Available: www.forcedimension.com/products/sigma-7/overview

[18] J. G. Dawes, Do data characteristics change according to the number of scale points used an experiment using 5 point, 7 point and 10 point scales, International journal of market research, vol. 51, no. 1, 2008.

[19] L. N. Verner and A. M. Okamura, Effects of translational and gripping force feedback are decoupled in a 4-degree-of-freedom telemanipulator, in Second Joint EuroHaptics Conference and Symposium on Haptic Interfaces for Virtual Environment and Teleoperator Systems (WHC07). IEEE, 2007, pp. 286?291.

[20] E. Theodorsson-Norheim, Friedman and quade tests: Basic computer program to perform nonparametric two-way analysis of variance and multiple comparisons on ranks of several related samples, Computers in biology and medicine, vol. 17, no. 2, pp. 85?99, 1987.